Age-Associated Proteomic Signatures and Potential Clinically Actionable Targets of Colorectal Cancer

Authors

Yanqiu Gong, Yu Liu, Tian Wang, Zhigui Li, Li Gao, Haining Chen, Yang Shu, Yuan Li, Heng Xu, Zongguang Zhou, and Lunzhi Dai

Correspondence

zhou767@163.com; lunzhi.dai@scu.edu.cn

In Brief

The incidence of early-onset colorectal cancer (CRC) has been increasing since 1990s, whereas the overall CRC frequency is declining. The underlying mechanisms of age-related clinical differences remain unknown. Here, we reported the proteomic signatures of CRC across age groups. Lots of proteins with adjusted intensities significantly correlated with age. Some proteins were verified as potential clinically actionable targets. This study identifies age-associated proteomic signatures and potential therapeutic targets of CRC and helps to make a precise decision on CRC treatment.

Graphical Abstract

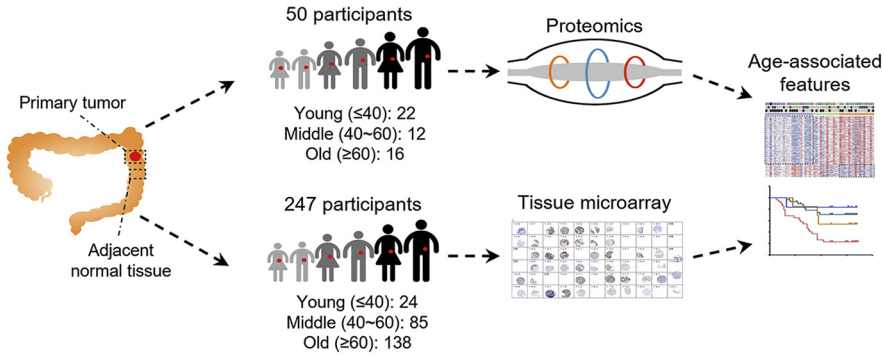

Highlights

- The proteomic signatures of early-onset CRC are disclosed.
- Alterations of some proteins between cancerous and normal tissues are age-correlated.
- NHP2, overexpressed in tumors especially in aged patients, predicts poor prognosis.
- Potential age-dependent druggable targets and their inhibitors are summarized.

2021, Mol Cell Proteomics *20*, 100115

https://doi.org/10.1016/j.mcpro.2021.100115

Age-Associated Proteomic Signatures and Potential Clinically Actionable Targets of Colorectal Cancer

Yanqiu Gong[1,‡], Yu Liu[1,‡], Tian Wang[2,‡], Zhigui Li[1,‡], Li Gao[1], Haining Chen[1], Yang Shu[1], Yuan Li[1], Heng Xu[1], Zongguang Zhou[1,*], and Lunzhi Dai[1,*]

The occurrence and prevalence of colorectal cancer (CRC) is closely associated with age. More than 90% of patients with CRC are diagnosed after 50 years of age. However, CRC incidence of young individuals has been increasing since 1990s, whereas the overall CRC frequency is declining. Distinct overall survival rates between young and aged patients with CRC have been established. Tremendous efforts have been made to clarify the underlying mechanisms of age-dependent clinical differences, but it still remains elusive. Here, we performed proteomic profiling of 50 patients with CRC and revealed proteomic signatures of CRC across age groups. Gene set enrichment analysis showed that distinct age-dependent clinical outcomes might mainly attribute to varied MYC targets V1/V2, E2F targets and G2M checkpoint gene sets, which were associated with cancer cell proliferation, cell apoptosis, tumor growth, and tumor metastasis. Multiple linear regression analysis revealed a large number of functional proteins, such as NOP2, CSE1L, NHP2, NOC2L and CDK1, with adjusted expression significantly correlated with age ($p < 0.05$). Among them, NHP2 is a core component of the telomerase complex associated with age. High NHP2 expression predicted poor overall survival, with a more significant correlation in aged patients with CRC. Knockdown of NHP2 significantly suppressed cancer cell proliferation. In addition, we revealed some age-related potential clinically actionable targets, such as PSEN1, TSPO, and CDK1, which might be more suitable for patients with late-onset CRC. Collectively, this study identifies age-associated proteomic signatures and potential therapeutic targets of CRC and may help make a precise decision on CRC treatment.

Colorectal cancer (CRC) is the second most deadly and the third most frequently occurring cancer worldwide (1). Obesity and overweight, physical inactivity, low-fiber diets, high red meat intake, suboptimal calcium intake, alcohol use, and smoking are common risk factors that are closely linked to the occurrence and progression of CRC (2). The risk of CRC rises dramatically in the populations with age over 50 years, and more than 90% of patients with CRC are diagnosed after 50 years of age. Although an overall decline in the incidence of CRC is observed in the past decades, a dramatic continuing rise of CRC, particularly the left colon or rectal cancers, happen in adolescent and young (Y) populations younger than 50 years (3). Whether patients with young-onset CRC have distinct biological behaviors and less-favorable prognosis is still debatable (4). The pathogenesis of young-onset CRC is well characterized in individuals with germline mutations. However, the understanding of molecular mechanisms of sporadic young-onset CRC is limited. The Y patients with CRC may have a unique molecular profile different from that of the aged (O) patients with CRC (5, 6).

Proteomics has recently been extensively used in elucidating the molecular mechanisms of occurrence and progression of cancer, providing opportunities to understand the inherent biology of cancer and take the precise treatments (7–10). Large integrative proteomic and genomic analyses of CRC have also been achieved, leading to identification of CRC subtypes, cancer antigens, drug targets, and critical signaling pathways associated with CRC progression (11–14). Although the proteomic landscape of O patients with CRC has been presented, the proteomic signatures of early-onset CRC are still less studied. The number of Y patients with CRC (age < 40 years) recruited in previous proteomics studies is still small, and only 4 Y patients out of 108 cases were described in Clinical Proteomic Tumor Analysis Consortium projects (https://proteomics.cancer.gov/programs/cptac). In this study, we performed proteomic profiling of paired tumors (T) and adjacent noncancerous tissues (N) from 50 patients with CRC

From the [1]Department of Gastrointestinal Surgery, National Clinical Research Center for Geriatrics and Department of General Practice, State Key Laboratory of Biotherapy, West China Hospital, Sichuan University, and Collaborative Innovation Center of Biotherapy, Chengdu, China; and [2]Life Science Mass Spectrometry Service Department, Thermo Fisher Scientific (China) Co, Chengdu, China

‡These authors contributed equally to this work.

*For correspondence: Lunzhi Dai, lunzhi.dai@scu.edu.cn; Zongguang Zhou, zhou767@163.com.

https://doi.org/10.1016/j.mcpro.2021.100115

and revealed distinct age-associated molecular signatures and potential therapeutic targets of CRC.

EXPERIMENTAL PROCEDURES

Declaration of Helsinki Principles

CRC samples were collected at West China Hospital with the approval of the research ethics committee (Permission number: 2020(374)). Informed consent was signed by the participants or families. Research was conducted according to the Declaration of Helsinki ethical principles.

Sample Collection

To avoid blood interference and protein degradation, the tissues were quickly washed with cold saline solution, frozen in liquid nitrogen, and then stored at −80 °C for later use. The adjacent noncancerous tissues were usually about 1 to 2 cm away from the margin of the tumors. The pathological sections of all the tissues were processed by the Department of Pathology, a laboratory accredited by the College of American Pathologists. The clinical information of all patients is included in supplemental Table S1. The colon tissues for immunohistochemical (IHC) analysis were obtained from the biobank of West China Hospital. The cohort contained 233 tumors and 209 adjacent nontumorous tissues. The clinical characteristics including TNM stage, grade, collection date, and lesion location, as well as the IHC results of NHP2 are included in supplemental Table S2. Patients with CRC suspected of Lynch syndrome or familial adenomatous polyposis were removed.

Protein Extraction and Digestion

CRC tissues were lysed in RIPA buffer (150 mM NaCl, 50 mM Tris (pH = 7.5), 1% NP-40 (v/v), 0.5% sodium deoxycholate (w/v), 25 mM nicotinamide, 10 mM sodium butyrate, 1× cocktail, 1× phosphatase inhibitors) and homogenized by gentleMACS Dissociators (Miltenyi Biotec GmbH) using the procedure "protein 01. 01". Then, the crude lysates were sonicated (model JY92-IIN, 227.5 W, 3 s on 10 s off, 5 min) and centrifuged (20,000*g*, 4 °C, 20 min). The concentrations of extracted proteins were measured by the Bradford protein assay (Bio-Rad). Fifty microgram of protein from each sample was reduced with 10 mM of tris (2-carboxyethyl) phosphine at 56 °C for 1 h, alkylated with 20 mM of iodoacetamide for 30 min to block the free cysteine residues, and precipitated with methanol/chloroform/water system. The enzymatic digestion was carried out overnight with trypsin at 37 °C in a 1:50 (w/w, trypsin/protein) ratio.

Isobaric Labeling

Tandem mass tag (TMT) reagents were equilibrated to room temperature (RT) and dissolved in anhydrous acetonitrile (ACN). Peptides were labeled with 10-plex TMT reagents according to the TMT 10plex reagents instructions (Thermo Scientific). After 1-h incubation at RT, 5% hydroxylamine was added to quench the reaction. Peptides labeled by different TMT labels were mixed and dried using SpeedVac. After reconstituted with 0.1% TFA, the peptides were desalted with C18 SPE column (Phenomenex) and fractionated on HPLC.

Peptide Fractionation

Desalted TMT-labeled peptides were fractionated by HPLC (agilent-1260, Agilent) on a 25-cm reversed-phase C18 column (HPH-C18 4 μM, 4.6 × 250 mm, Poroshell, Agilent, 40 °C column temperature, 214-nm UV detection). The separation was performed at a flow rate of 1 ml/min with mobile phase buffer A (98% water with 2% ACN, 10 mM ammonium formate, pH = 10) and mobile phase buffer B (90% ACN with 10% water, 10 mM ammonium formate, pH = 10). A standard 120-min LC gradient run was used: 0 to 90 min, 3% to 35% buffer B; 90 to 105 min, 35% to 60% buffer B; 105 to 115 min, 60% to 100% buffer B; 115 to 120 min, 100% to 3% buffer B. The obtained 120 fractions were combined into 40 parts, vacuum-centrifuged to dryness, and desalted with C18 ZipTip before LC-MS/MS analysis.

MS Analysis

After desalting, the peptide samples were loaded onto a 100 μm (inner diameter) × 2 cm (length) trap column and a 75 μm (inner diameter) × 15 cm (length) analytical column, which were packed with C18 resin (DIKMA) in-house, and LC-MS/MS analysis was executed using an EASY-nLC 1000 nanoflow LC instrument coupled to a Q Exactive Plus Quadrupole-Orbitrap mass spectrometer (Thermo Fisher Scientific). Peptide samples were analyzed with a 65-min gradient from 6 to 95% buffer B (95% ACN and 0.1% formic acid) at a flow rate of 300 nl/min. The data-dependent acquisition was performed in a positive-ion mode. Survey full-scan MS spectra (from m/z 350–1600) were acquired in the Orbitrap with resolving power of 70,000 at m/z = 200. The automatic gain control value setting was set at 3e6, with maximum fill times of 20 ms. For MS/MS scans, the top 15 most intense parent ions were selected with a 0.6 m/z isolation window and fragmented with a normalized collision energy of 30%. The automatic gain control value for MS/MS was set to a target value of 1e5, with a resolution of 35,000 and a maximum fill time of 100 ms. Parent ions with a charge state of z = 1 or 8 or with unassigned charge states were excluded for fragmentation. A dynamic exclusion period for the data-dependent scan was 50 s.

MS Data Analysis

All the raw files were searched against the Swiss-Prot human protein sequence database (updated on 01/2017; 20,413 protein sequences) by using MaxQuant (version 1.6). Searches were carried out with a precursor peptide mass tolerance of 10 ppm and a fragment ion mass tolerance of 0.02 Da. Quantification was filtered by min reporter precursor intensity fraction at 75%. The minimum amino acid length was set to 6. Two missed trypsin cleavages were allowed. Peptides were not nested within another longer peptide. Cysteine carbamidomethylation was set as a fixed modification. Oxidation of methionine and protein *N*-terminal acetylation were set as variable modifications. Proteins with a false discovery rate (FDR) <1% at both protein and peptide levels, and at least two peptides were chosen for further data processing. The MS raw data, the MaxQuant software, and the whole txt files have been deposited into the ProteomeXchange Consortium (http://proteomecentral.proteomexchange.org) *via* the iProX partner repository (15), with a dataset identifier of PXD022714.

Experimental Design and Statistical Rationale

Fifty paired CRC samples used in our proteomics were divided into 12 TMT batches. TMT labeling information is shown in supplemental Table S3. The proteomic data of different batches including technical replicates are included supplemental Table S4. The total intensities of the samples in the same batch of TMT-based quantification were first normalized after removing the contaminant and reverse hits. Then, the protein intensities of the tumor were normalized to the adjacent nontumorous tissue to get the protein ratios (T/N), which were termed adjusted protein intensities. The adjusted protein intensities of all tumor tissues were then combined into a larger table (supplemental Table S5). To ensure the inference stringency of proteins quantified in our study, proteins quantified in more than 66.7% patients with >2 peptides identified in at least one batch were used for subsequent data mining, according to the neXtProt Unitypicity Checker (16). Proteins with ratios of T/N >1.5 (or <0.67) and q values <0.05 (Wilcoxon rank-sum test) were

defined as significantly differentially expressed proteins in tumors (supplemental Table S6). Enriched processes and pathways using the differentially expressed proteins between tumors and normal tissues are provided in supplemental Table S7. The significantly differentially expressed proteins between tumors and normal tissues in Y and O groups are, respectively, shown in supplemental Table S8. Enriched biological processes using differentially expressed proteins in Y and O CRC groups are included in supplemental Table S9. The proteins with adjusted intensities between Y and O patients more than 1.5-fold were considered as age-associated proteins (Wilcoxon rank-sum test, FDR <0.05) (supplemental Table S10). Because some patients in the validation cohort lost to follow-up, the overall survival (OS) of the remaining 191 patients was calculated to determine the clinical significance of NHP2. The OS was the time calculated from diagnosis to dead or censored, the longest survival period in the validation cohort was 69 months.

Bioinformatics and Statistical Analysis

The R package Rtsne was used to visualize the outliers of all patients with CRC and separation of age-dependent groups. Gene set enrichment analysis (GSEA) was used for hallmark pathway enrichment. The reference lists of colon-specific proteins and marker proteins were downloaded from the Human Protein Atlas. The reference list of transcription factors was from the *Cell* article (17). Correlation of adjusted protein intensities with age was assessed with linear models using multiple regression (numerical variables) analysis in R. To determine the linear correlation of adjusted protein intensities to age, we used the following linear model:

$$\text{Age} \sim \text{adjusted protein intensities} + \text{sex} + \text{lesion location} + \text{TNM stage}$$

The variables including adjusted protein intensities, sex, lesion location, and TNM stage were used in the regression model. The relative abundance of immunoblots was calculated by ImageJ. The QuPath was used for IHC analysis. The other R packages including pheatmap, ggplot2, dplyr, readxl, ggrepal, and reshape were used for data processing and presentation. The OS was analyzed in GraphPad Prism (V.8.0).

IHC Staining

CRC tissue microarray was obtained from West China Hospital biobank of Sichuan University. Formalin-fixed and paraffin-embedded tumor tissues were sliced into 4-μm sections for IHC staining. Tissue sections were successively deparaffinized in xylene, rehydrated with graded ethanol, and rinsed in distilled water. Antigen retrieval was performed with Tris/EDTA at pH 9.0 and 140 °C. The sections were blocked with 4% bovine serum albumin in PBS and incubated with NPH2 antibody (CAT# ab180498, Abcam) at 4 °C overnight after the treatment with 3% H_2O_2 in methanol for 15 min at 37 °C to block endogenous peroxidases. Then, the sections were washed, and Image-Pro Plus 6.0 software was used for evaluating and scoring the expression of NHP2 (supplemental Table S2).

Cell Culture and Transfection

Human CRC cell lines HT29 and HCT116 were cultured in Dulbecco's modified Eagle's medium (DMEM) (#C11995-065, Gibco). SW620 was cultured in RPMI 1640 medium (1640) (#10270-106, Gibco). The DMEM and 1640 were supplemented with 10% (v/v) fetal bovine serum (#SFBE, NATOCOR), 100 U/ml penicillin, and 100 μg/ml streptomycin (#15140-122, Gibco) before use. The cell lines were cultured at 37 °C in a humidified incubator with 5% CO_2. To produce the lentivirus, lentiviral vector of pLKO.1-derived plasmid for NHP2 and NOC2L knockdown, packaging plasmid pCMV-dR8.2 dvpr and envelope plasmid pCMV-VSVG were cotransfected into 293T cells (System Biosciences). The concentration of viruses was measured by the PEG-it Virus precipitation solution. The viruses were then used for cell infection. After 72 h, the stable cells were selected with 2 μg/ml of puromycin.

shRNA1 for NHP2: CCGGGTCATGTGTGAGGACCGAAATCTCGAGATTTCGGTCCTCACACATGACTTTTT.

shRNA2 for NHP2: CCGGGAAGCTCTACAAATGCATCAACTCGAGTTGATGCATTTGTAGAGCTTCTTTTT.

shRNA1 for NOC2L: CCGGCCCTGAGATCAAACGAAGGAACTCGAGTTCCTTCGTTTGATCTCAGGGTTTTTTG.

shRNA2 for NOC2L: CCGGGCCTTTCATCCTGGAGATGTTCTCGAGAACATCTCCAGGATGAAAGGCTTTTTG.

Western Blotting Analysis

CRC tissues and cultured cells were lysed with RIPA buffer (NaCl 150 mM, 50 mM Tris (pH = 7.5), NP-40 1% (v/v), sodium deoxycholate 0.5% (w/v), nicotinamide 25 mM, sodium butyrate 10 mM, 1× cocktail, 1× phosphatase inhibitors). The protein concentrations were measured using the Bradford assay. The protein samples were then separated in 10% SDS-PAGE and transferred onto PVDF membranes. The membranes were blocked with 4% nonfat dry milk in PBS with 0.1% Tween 20 and incubated with NHP2 antibody (SANTA Cruz, sc-398430) (1:2000), CDK1 antibody (ab13327, Abcam) (1:5000), NOP2 antibody (sc-398884, Santa Cruz) (1:1000), CSE1L antibody (ab151546, Abcam) (1:2500), NOC2L antibody (ImmunoWay, YT3160) (1:2000), or actin antibody (CAT# ET1701-80, HUABIO) (1:5000) overnight at 4 °C. Then, the membranes were washed and incubated with the secondary antibody at RT for 1 h. The specific bands were detected using Immobilon Western HRP Substrate (Millipore). The relative protein intensity was calculated by ImageJ software.

MTT Assay and Colon Formation

MTT (3-(4,5-dimethylthiazol-2-yl)-2,5-diphenyltetrazolium bromide) was used for cell proliferation assay. About 3×10^3 cells were seeded on 96-well plates, and the cell numbers were counted every day. The numbers of SW620 and HT29 cells were continuously counted for 5 days and 4 days, respectively. Then, 10 μl of the MTT buffer was added to each well and incubated for 4 h. After removing the solution, 150 μl DMSO was added and thoroughly dissolved. The absorbance was measured at 570 nm using Synergy H1 (BioTek). Each time point had four repeats, and the experiment was repeated for three times under the same conditions. The data were analyzed using GraphPad Prism 8 software. For colony-formation assay, cells were seeded on 6-well plates in 1500 cells/well and cultured until the visualization cell colonies appeared. The colonies were fixed by 4% paraformaldehyde for 30 min and then stained with hematoxylin for another 30 min.

RESULTS

Proteomic Profiling

Of the 50 patients with CRC, 22 were Y (<41 years old), 12 were middle aged (41–60 years old, M), and 16 were O (>60 years old) (supplemental Table S1 and supplemental Fig. S1). Quantitative proteomics was performed using TMT-based isobaric labeling strategy followed by LC-MS/MS analysis (supplemental Table S3). To evaluate the reliability of measurements, eight pairs of tissues were analyzed in duplicate. The median CV of the measured protein ratios (T/N) between duplicates were less than 0.1 (Fig. 1*A*), and the correlation between duplicates was from 0.8 to 0.9 (supplemental Fig. S2). Besides, t-distributed stochastic neighbor embedding was used to display our high-dimensional datasets of 50 patients in two dimensions, and

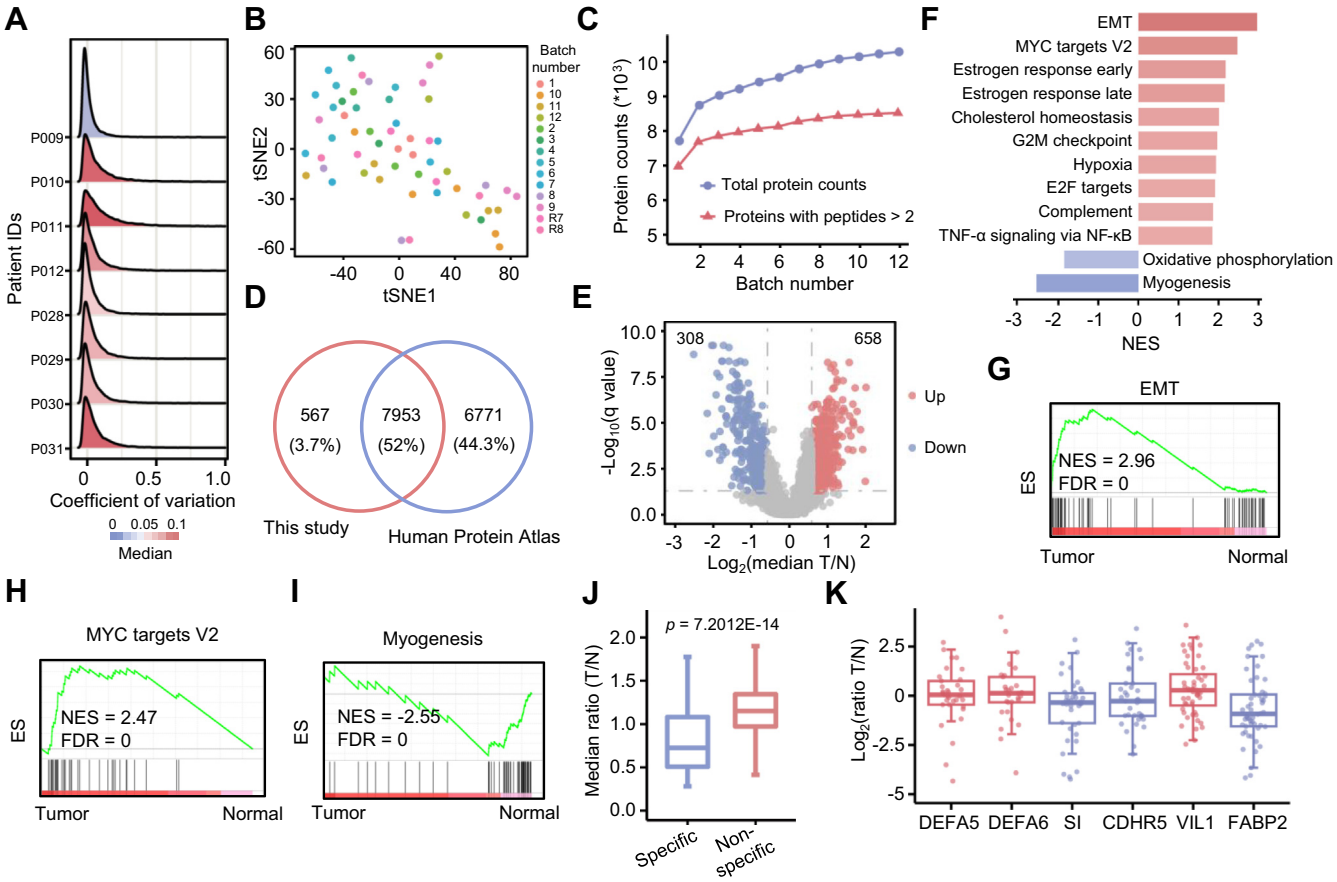

FIG. 1. **Quantitative proteomic profiling of CRC.** *A*, the median CV of measured protein ratios (T/N) between duplicates of eight pairs of CRC samples. *B*, t-SNE plot of different batches of samples and replicates. The R7 and R8 represent the technical replicates of batches 7 and 8, respectively. *C*, cumulative number of identified proteins. *D*, Venn diagram shows the number of proteins overlapped with the identified intestinal proteins listed in the Human Protein Atlas database. *E*, volcano plot shows 658 upregulated and 308 downregulated proteins in tumors (ratio(T/N) > 1.5 or < 0.67, and Wilcoxon rank-sum test, FDR < 0.05). *F*, GSEA preranked hallmark analysis of 966 differentially expressed proteins. NES represents the normalized enrichment score. *G–I*, top significant hallmark pathways in tumorous or nontumorous tissues. ES represents the enrichment score. *J*, box plot shows the overall changes of specific and nonspecific colon signature proteins in tumors. *K*, the changes of representative proteins associated with intestinal functions. CRC, colorectal cancer; FDR, false discovery rate; GSEA, gene set enrichment analysis; t-SNE, t-distributed stochastic neighbor embedding.

both obvious outliers and TMT batch effect were not observed (Fig. 1*B* and supplemental Fig. S3). These analyses collectively indicate the high reliability of proteomics data.

In total, we identified 10,288 proteins with 1% FDR at both protein and peptide levels, and 8524 proteins had more than two peptides (Fig. 1*C* and supplemental Table S5). Compared with the identified intestinal proteins mapped in Human Protein Atlas (18), 7953 proteins overlapped (Fig. 1*D*). Among all identified proteins, 4413 proteins were quantified in all 50 patients, representing the core components of proteome. 6040 proteins quantified in more than 66% of CRC cases with at least two peptides were used for subsequent data mining. A total number of 966 proteins were significantly differentially expressed (Wilcoxon rank-sum test, FDR <0.05, ratio (T/N) >1.5 or <0.67) between paired tumorous and nontumorous tissues (Fig. 1*E*). Among them, 658 proteins were upregulated and 308 proteins were downregulated in tumors (Fig. 1*E* and supplemental Table S6). GSEA showed that epithelial mesenchymal transition and MYC targets V2 were most significantly upregulated in tumors, whereas myogenesis and oxidation phosphorylation were significantly reduced (Fig. 1, *F–I*). Notably, colon-specific proteins annotated in the Human Protein Atlas were dramatically decreased (Fig. 1*J*), and many proteins related to intestinal functions such as microvilli organization and digestion were lost in tumors (Fig. 1*K*). For example, FABP2 is thought to be involved in fatty acid absorption (19), and SI plays an important role in the final stage of carbohydrate digestion (20). The above results indicate that the loss of colon signature proteins is an important feature of CRC.

Age-Associated Proteomic Signatures

The normal protein levels vary greatly among individuals and are associated with phenotypic variations (21). More dramatic difference of protein expression between the normal

and tumorous tissues makes the protein more likely to be a therapeutic target. An ideal target for cancer therapy would be a protein that is only present in tumor but not in healthy cells, which leads to more effective therapies with less side effects (22). To reduce the expression variations among patients and figure out the proteins with most significant expression difference between the normal and tumor tissues, adjusted protein intensity of the tumor, which was obtained by adding the protein expression in the tumor to that in the corresponding adjacent non-tumorous tissue, was used for the subsequent data mining. Based on the adjusted intensities of 6040 proteins, the 50 patients with CRC were clearly separated into age-dependent three groups using orthogonal partial least squares-discriminant analysis algorithm (Fig. 2*A*). Advanced malignant cancer stages are known to activate certain signal pathways such as metastasis. To exclude the influence of cancer stages on the screening of differentiating proteins, we calculated the stage difference by the chi-square test (supplemental Fig. S4), and no significant stage difference among Y, M, and O subcohorts was observed, indicating that the age-associated classification and analysis in our study was independent on the clinical stage.

Subsequently, we examined the differences between cancerous and adjacent nontumorous tissues in the Y and O groups, respectively. Volcano plot of Y patients with CRC showed that there were 190 upregulated and 257 downregulated proteins in tumors (ratio (T/N) >1.5 or <0.67, and Wilcoxon rank-sum test, FDR <0.05) (supplemental Fig. S5*A* and supplemental Table S8). Enrichment analysis of differentially expressed proteins revealed that extracellular matrix organization, protein hydroxylation, collagen metabolic process, and other processes were upregulated in tumors, whereas muscle contraction as expected from normal colon histology, biological oxidation, and metabolism-related processes were downregulated in tumors (supplemental Fig. S5*B* and supplemental Table S9). In O patients with CRC, 2046 upregulated and 440 downregulated proteins were identified in tumors (ratio (T/N) >1.5 or <0.67, and Wilcoxon rank-sum test, FDR <0.05) (supplemental Fig. S5*C* and supplemental Table S8), indicating that the protein expression differences between cancerous and nontumorous tissues were much larger in O patients with CRC. The 2046 upregulated proteins were significantly enriched in rRNA processing, RNA splicing, RNA catabolic process, and other processes related to ribosome biogenesis, whereas the 440 downregulated proteins were significantly enriched in response to wounding, DNA-templated transcription, and elongation (supplemental Fig. S5*D* and supplemental Table S9).

GSEA was next performed with the adjusted intensities of 6040 proteins to reveal the proteomic differences between Y and O patients. We found that the proteins with big differences between tumors and normal tissues in O patients were associated with MYC targets V1/V2, E2F target, G2M checkpoint, DNA repair, unfolded protein response, and mTORC1 signaling (Fig. 2*B*). In particular, SNRPD1, TRA2B, NOP16, NHP2, HNRNPA2B1, EIF1AX, SF3B3, PRL18, and NOP2 belonging to MYC targets V1, NOP16, SERBP1, PPAN, DCTPP1, TOCF1, HK2, and NOC4L associated with MYC targets V2, TRA2B, DCTPP1, CSE1L, HMGA1, CDK1, NUP205, RBBP7, RFC3, and PNN featured in E2F targets, as well as SNRPD1, TRA2B, HMGA1, CDK1, EWSR1, CUL4A, and KIF11 linked to G2M checkpoint were the key molecules with much higher adjusted intensities in O patients with CRC (Fig. 2*C*). Moreover, we found that proteins belonging to extracellular space and zinc ion binding showed bigger differences between tumors and normal tissues in Y patients (Fig. 2*D*).

We next screened the proteins with significantly different adjusted intensities between Y and O patients. 254 proteins with higher adjusted intensities in O patients with CRC mainly involved in metabolism of RNA, ribosomal large subunit biogenesis, neutrophil degranulation, translation, extracellular matrix organization, and nuclear transport, whereas 65 proteins with lower adjusted intensities in O patients with CRC were closely related to human complement system and NABA core matrisome (Wilcoxon rank-sum test, FDR < 0.05, and ratio (O/Y) >1.5 or <0.67) (Fig. 2*E* and supplemental Table S10). Multiple linear regression analysis of the 319 proteins revealed 208 proteins such as NOP2, CCDC51, NOC2L, NOL7, CDK5RAP1, RRP1B, CSE1L, NHP2, PPAN, and CDK1 significantly positively correlated with age (Wilcoxon rank-sum test, FDR < 0.05) (Fig. 2*F*). In contrast, only 20 proteins with adjusted intensities significantly negatively correlated with age (Wilcoxon rank-sum test, FDR < 0.05) (supplemental Fig. S6). Taken together, the results indicate that bigger proteomic difference between cancerous and adjacent normal tissues is a feature of O patients with CRC.

Validation of Age-Associated Differentially Expressed Proteins

We next verified the proteomic data by Western blots in the same samples (Fig. 3, *A–E*). Consistent with the proteomic data, the adjusted intensities of NOP2, NOC2L, CSE1L, NHP2, and CDK1 was dramatically higher in tumors of O patients (Fig. 3, *F–J*). NOP2 is ribosomal RNA methyltransferase and plays important roles in late G1 and S phases of cell cycle to regulate the synthesis of DNA and cell division. Higher expression of NOP2 is linked to a more rapidly proliferating tumor and correlates with unfavorable prognosis (23). CSE1L functions in the mitotic spindle checkpoint and assures genomic stability during cell division. It is highly abundant in proliferating cells and malignancies such as breast and colon cancers but lowly expressed in quiescent cells (24, 25). CDK1 is a highly conserved protein that functions as a serine/threonine kinase. Previous studies have shown that CDK1 involves in the progression of multiple types of cancers, and the upregulation of CDK1 is associated with reduced survival time (26, 27). NOC2-like protein (NOC2L), which binds directly

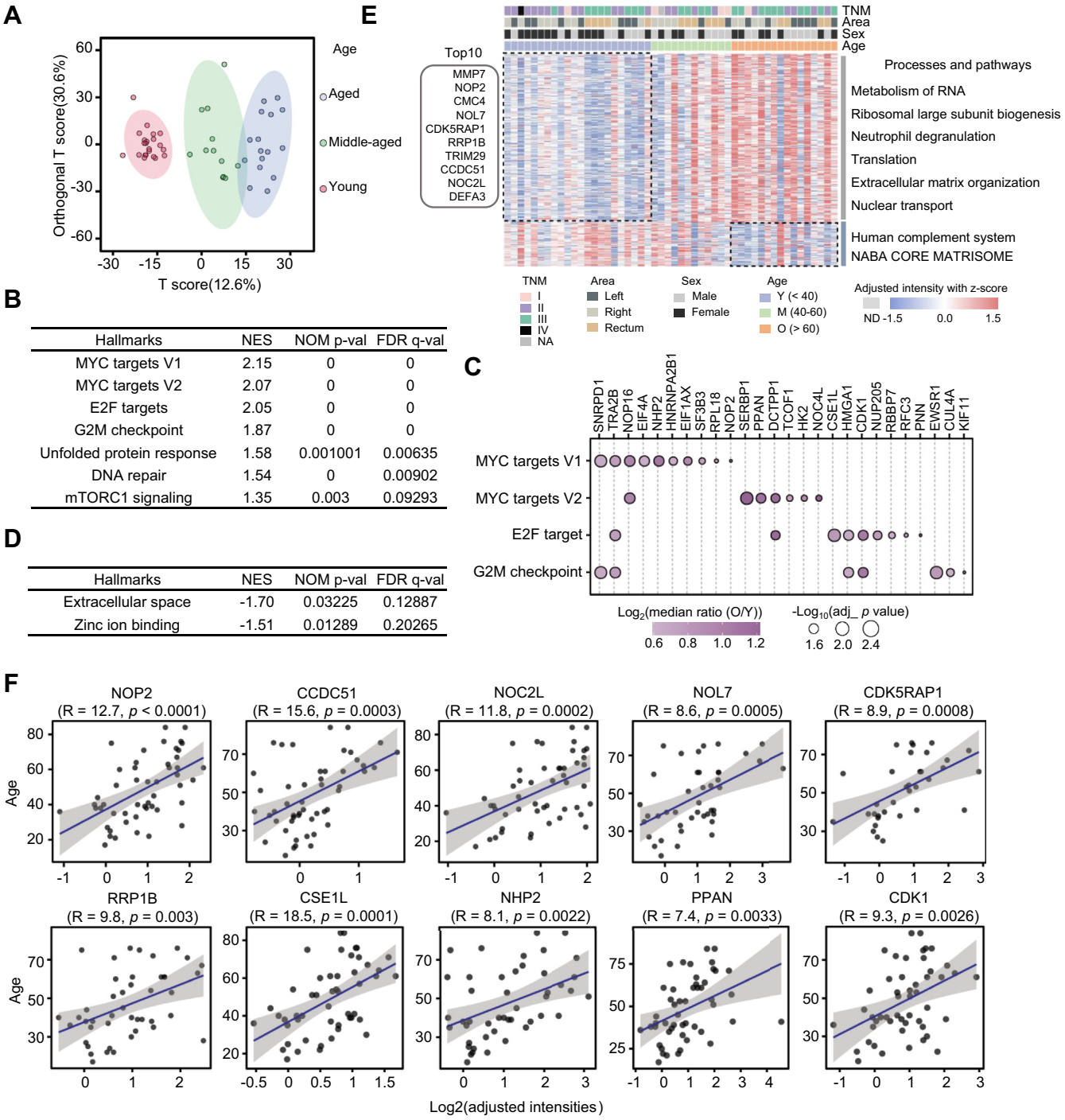

FIG. 2. **Age-associated proteomic signatures.** *A*, orthogonal partial least squares-discriminant analysis (OPLS-DA) of young, middle-aged, and aged CRC groups. *B*, GSEA of 6040 proteins identified hallmarks in aged patients with CRC (FDR q < 0.25, and NOM p < 0.05). NOM represents the nominal p value. *C*, the plot shows changes of proteins belonging to the top four enriched hallmark pathways shown in panel *B*. The protein ratios between young and aged patients with CRC were calculated with median-adjusted protein intensities. *D*, hallmarks enriched in young patients with CRC (FDR q < 0.25, and NOM p < 0.05). *E*, enrichment analysis of proteins with adjusted intensities significantly different between young and aged patients with CRC (Wilcoxon rank-sum test, FDR < 0.05, and ratio (O/Y) > 1.5 or < 0.67). The TNM stage, lesion location, sex, and age of patients are annotated above the heatmap. The heatmap depicts the adjusted intensities of proteins with log2-transformation. Biological functions of these proteins are shown at the *right* of the heatmap. *F*, representative differentially expressed proteins showing significant linear correlation with age. R represents the protein coefficient of linear regression analysis. The p value means the significance of linear correlation. CRC, colorectal cancer; FDR, false discovery rate; GSEA, gene set enrichment analysis.

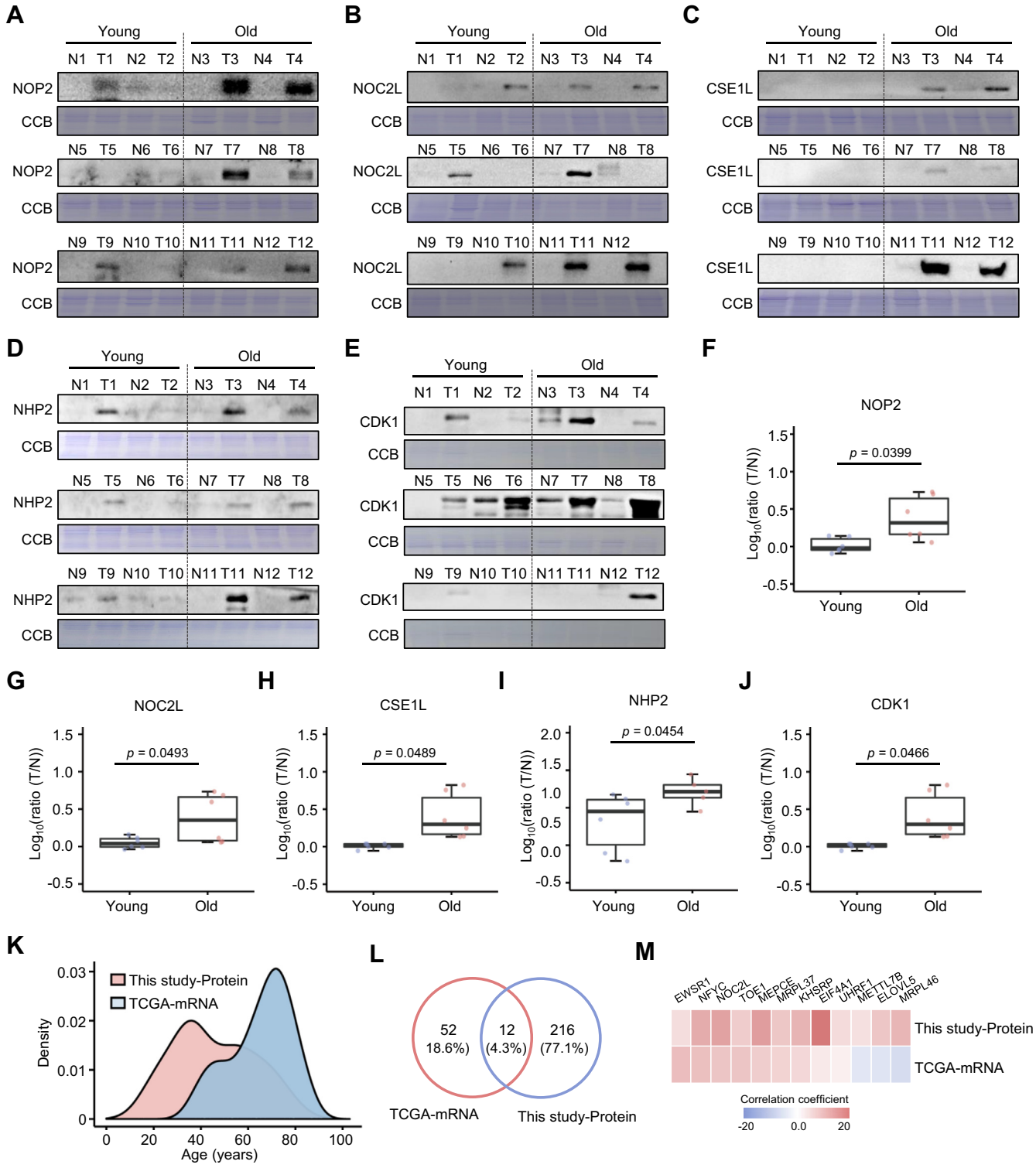

FIG. 3. **Validation of age-associated differentially expressed proteins.** Immunoblots showed the expression of NOP2 (*A*), NOC2L (*B*), CSE1L (*C*), NHP2 (*D*), and CDK1 (*E*) in the tumorous and paired nontumorous tissues of young and aged patients with CRC. The statistics of the relative protein expression of NOP2 (*F*), NOC2L (*G*), CSE1L (*H*), NHP2 (*I*), and CDK1 (*J*) are shown in panels *A*–*E*. *K*, density plot displaying the age distribution of patients from proteomics (n = 50) and TCGA transcriptomics (n = 50). *L*, the overlapped genes/proteins with significantly linear correlation with age (Wilcoxon rank-sum test, *FDR* < 0.05, median ratio (O/Y) > 1.5 or < 0.67, and *p* value of linear correlation < 0.05). *M*, the heatmap of multiple linear regression coefficient for the overlapped 12 proteins shown in panel *L*. O, aged; Y, young.

to the tumor suppressor p53, has been proved as an oncogene in pancreatic cancer (28). To our best knowledge, the functions of NOC2L is still less understood. By knocking down NOC2L in HCT116 cell line, we found that the clone formation and cell viability were significantly suppressed, suggesting the role NOC2L in promoting the cancer cell proliferation (supplemental Fig. S7).

We further compared our proteomics data with The Cancer Genome Atlas (TCGA) transcriptomics data, although only few Y patients with CRC were included in TCGA database (Fig. 3*K*). Multiple linear regression analysis of TCGA transcriptomics data identified 64 critical genes with adjusted intensities linearly correlated with age, of which 12 genes overlapped with the proteins showing linear correlation with age (Fig. 3*L*). Among the 12 genes/proteins, the adjusted protein and mRNA intensities of EWSR1, NFYC, NOC2L, TOE1, MEPCE, MRPL37, KHSRP, EIF4A1, and UHRF1 were positively correlated, whereas those of METTL7B, ELOVL5, and MRPL46 were negatively correlated (Fig. 3*M*). As we know, the protein–RNA correlation in tumors is usually around 0.4 to 0.5 (9); our result is consistent with previous reports, suggesting the reliability of our findings.

Clinical Significance of Telomerase Component NHP2 in Patients With CRC Across Age Groups

Telomerase is a large ribonucleoprotein complex responsible for extending the telomeres of chromosomes, which usually decreases in senescence somatic normal cells (29, 30). Restrained or shortened telomeres have been widely used for cancer therapeutics (31, 32). NHP2 is a critical component of telomerase (29, 30). Mutations of NHP2 may cause the premature aging syndrome dyskeratosis congenita (33). However, the clinical significance and roles of NHP2 in cancer was completely unknown in CRC. Proteomics results showed that NHP2 was significantly upregulated in tumors, especially in tumors of O patients with CRC, which was further confirmed by Western blots (Fig. 3, *D* and *I*). To identify the clinical significance of NHP2, another CRC cohort including 442 colon tissues was used for IHC analysis. We found that NHP2 was remarkably upregulated in the tumors (n = 233) compared with the adjacent nontumorous tissues (n = 209) (Fig. 4, *A* and *B*). The NHP2 levels in 131 tumors of O patients were higher than that in 23 tumors of Y patients (Fig. 4*C*). Survival analysis showed that patients with CRC with higher NHP2 expression in tumors had a significantly lower 5-year OS (p = 0.0115) (Fig. 4*D*). In the O cohort, the patients with higher NHP2 expression in tumors had even worse prognosis (p = 0.0034) (Fig. 4*E*), implying that NHP2 plays critical roles in the progression of CRC in an age-dependent manner. To further verify the role of NHP2 in CRC, we knocked down NHP2 in two CRC cell lines (SW620 and HT29) (Fig. 4*F*) and found that the cell viability and clone formation were significantly suppressed (Fig. 4, *J–H*). The above results collectively showed that NHP2 was an unfavorable oncogene in CRC, especially in late-onset CRC.

Other Differentially Expressed Functional Proteins Linearly Correlated With Age

The expression or activity of transcriptional factors is strictly controlled under normal conditions. However, during the tumorigenesis, many transcriptional factors, such as c-MYC and STAT3, become oncogenic and drive the occurrence and progression of CRC (34). To date, age-associated profile of transcriptional factors in CRC has never been described. In the multiple linear regression, we identified 28 transcriptional factors such as NOP2, GTF2I, CUL4A, NOC3L, NOC4L, and LRRFIP2 with adjusted intensities significantly correlated with age (Fig. 5), of which CUL4A displayed the most significant correlation with age. CUL4A is known to promote proliferation and metastasis of CRC cells, and high expression of CUL4A predicts poor prognosis (35). CUL4A showed higher adjusted expression in O patients with CRC, suggesting that CUL4A might play a more significantly role in O patients. Besides, KIF11 (36), ACLY (37), SF3B3 (38), and UHRF1 (39) were also important factors that regulated the CRC progression. Although most transcriptional factors showed elevated levels in tumors and higher adjusted intensities with age, we still observed an exceptional transcriptional factor LRRFIP2 downregulated in CRC tumors, and the adjusted expression of LRRFIP2 was negatively correlated with age. LRRFIP2 is an NLRP3-associated protein and serves as an inhibitor for NLRP3 inflammasome activation (40). The activation of NLRP3 inflammasome drives tumorigenesis in some types of cancers, although its role in malignant progression remains controversial (41). LRRFIP2 showed much lower adjusted intensities in O patients with CRC, indicating a significant role of NLRP3 inflammasome activation during CRC progression in O patients.

Compared with the databases of oncoproteins (http://ongene.bioinfo-minzhao.org/), and tumor suppressors (https://bioinfo.uth.edu/TSGene/), we identified eight oncoproteins such as CDK1, HMGA1, RFC3, and EWSR1, as well as eight tumor suppressors such as ZNF185, SMARCA4, CASP8, and PNN significantly correlated with age (Fig. 5). Interestingly, we found that these “tumor suppressors” might still have functions of oncoproteins. For example, ZNF185 is a liver metastasis–associated factor in patients with colon cancer, and the expression of ZNF185 is an independent indicator of liver metastasis (42). PNN (pinin) could promote cell proliferation and tumor metastasis of CRC through activating the EGFR/ERK signaling pathway (43). The loss of CASP8 is nonetheless a rare event in CRC, and the elevated expression of CASP8 in tumors has been observed (44). SMARCA4 is mostly overexpressed in tumors, and high SMARCA4 expression is associated with poor prognosis in many types of tumors (45).

Age-Associated Potential Clinically Actionable Targets for CRC Treatment

To investigate the clinical implications of age-associated proteomic signatures, we focused on the proteins with

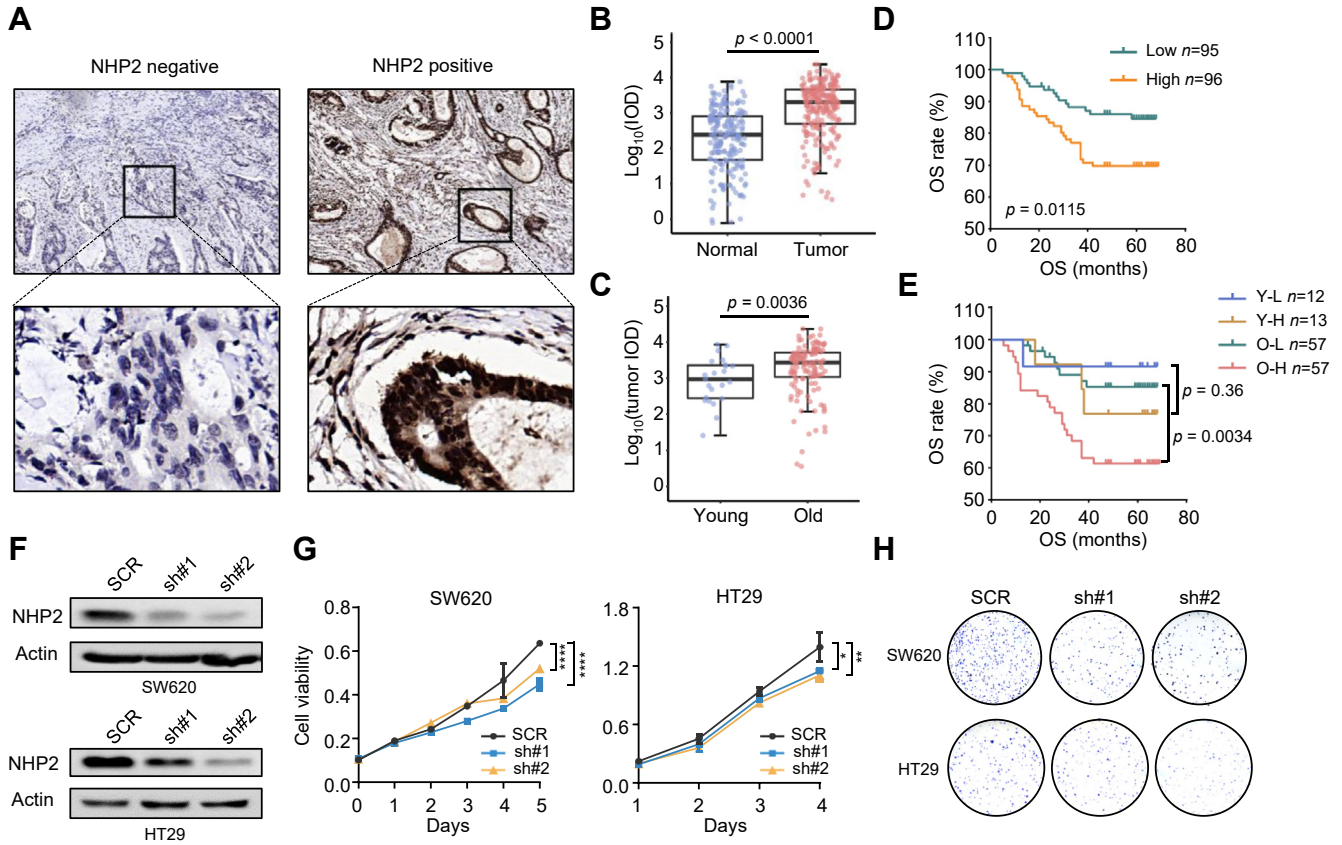

FIG. 4. **Clinical significance of telomerase component NHP2 in patients with CRC across age groups.** *A*, representative IHC images for NHP2 negative and positive of CRC tumors. *B*, comparison of NHP2 expression in tumors and adjacent normal tissues based on the integrated option density (IOD) with log10 transformation. The IOD was calculated using Image-Pro Plus 6.0 software. *C*, comparison of NHP2 expression in tumors of young and aged patients based on the IOD with log10 transformation. *D*, the relationship between NHP2 expression and OS. The *p* value was calculated by using the log-rank test. *E*, comparison of OS rates among young patients with high NHP2 expression, young patients with low NHP2 expression, aged patients with high NHP2 expression, and aged patients with low NHP2 expression. *F*, immunoblotting validation of the knockdown of NHP2. *G*, the influence of NHP2 knockdown on cancer cell proliferation. *H*, the influence of NHP2 knockdown on colony formation. CRC, colorectal cancer; IHC, immunohistochemical; OS, overall survival.

adjusted intensities linearly correlated with age. By referring to known drug targets with Food and Drug Administration–approved drugs or candidate drugs in clinical trials, we identified 18 clinically actionable proteins whose adjusted intensities were linearly correlated with age ($p < 0.05$) (Fig. 6), of which eight proteins including PTGES, CDK1, CD38, PSEN1, KIF11, HK2, ATM, and CYP51A1 were with fold changes of median-adjusted intensities more than 1.5 between Y and O patients with CRC (Fig. 6). PSEN1 is a subunit of γ-secretases participating in the activation of the Notch signaling pathway (46). Dysregulation of Notch signaling might be associated with CRC tumorigenesis (47). As normal aging, Notch signaling is enhanced in certain types of stem cells. Much higher adjusted PSEN1 intensities were observed in most O patients with CRC, indicating that PSEN1 might be a candidate therapeutic target for the O patients with CRC. CDK1 is a key regulator of mammalian cell proliferation and initiates the onset of mitosis (48). Inhibition of CDK1 significantly induced apoptosis and reduced viability of MYC-dependent cells (49). Our proteomic results showed that MYC targets V1/V2 genes were highly expressed in CRC tumors, especially in the tumors of O patients (Figs. 1*F* and 2*D*), suggesting that CDK1 might be a candidate target for CRC treatment in the elderly. In particular, CD38 and TSPO had Food and Drug Administration–approved drugs (Fig. 6). Daratumumab and Isatuximab are mAbs targeting CD38 to treat multiple myeloma cells. By targeting CD38, Daratumumab and Isatuximab inhibit cancer cell growth, survival, and adhesion and also play a role in T-cell activation (50). High expression of CD38 in patients with CRC, especially in O patients, probably makes Daratumumab and Isatuximab as choices for the treatment of CRC. TSPO is a five-transmembrane domain protein responsible for the translocation of cholesterol. The expression level of TSPO is a sensitive biomarker linked to

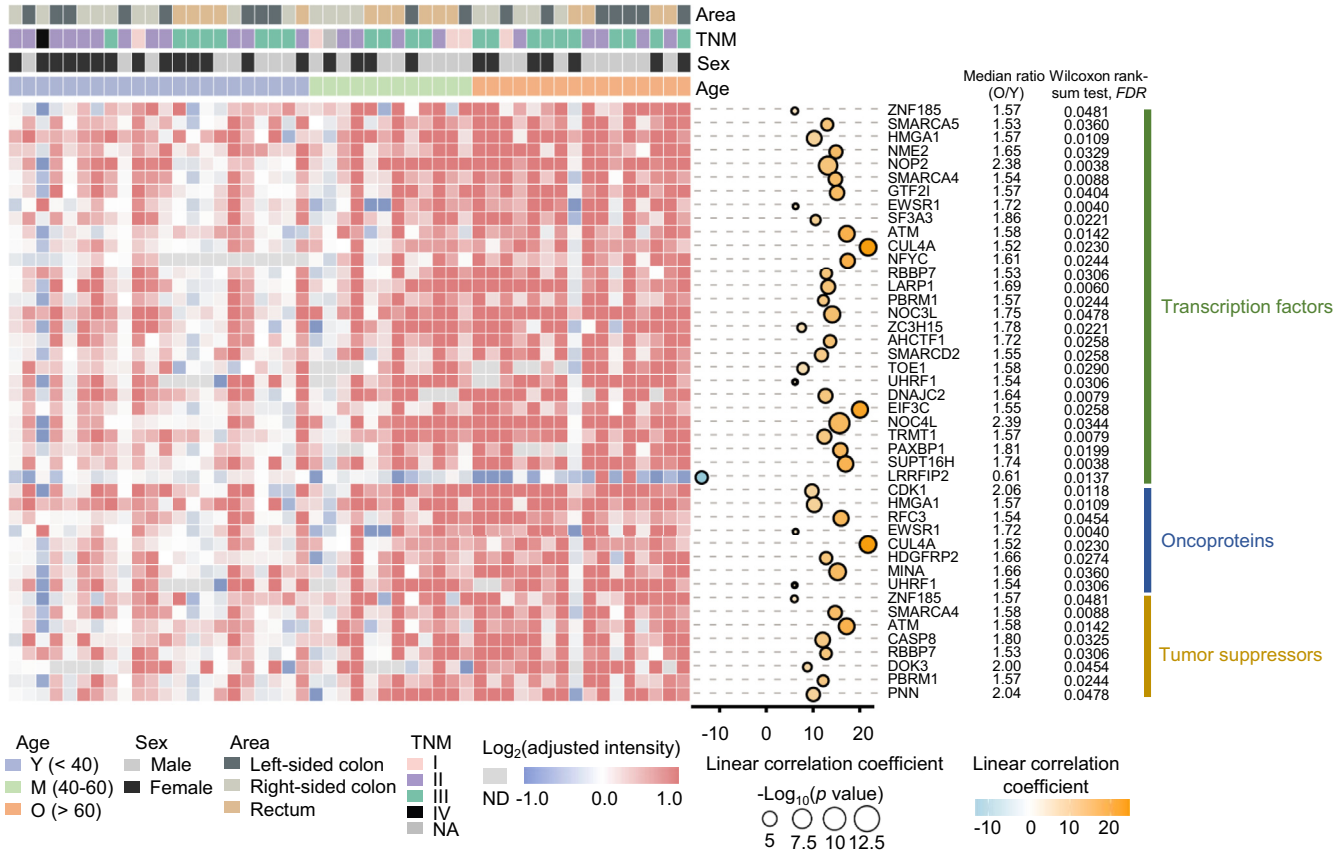

FIG. 5. **Age-associated functional proteins.** The age-associated differentially expressed transcription factors, oncoproteins, and tumor suppressors were present (Wilcoxon rank-sum test, FDR < 0.05, median ratio (O/Y) > 1.5 or < 0.667, and $p < 0.05$ for linear regression). The TNM stage, lesion location, sex, and age of patients are annotated above the heatmap. The heatmap depicts the adjusted intensities of functional proteins with log2 transformation. The bubble chart describes the coefficients with age. FDR, false discovery rate; O, aged; Y, young.

brain damage, neurodegeneration, inflammation, and reactive gliosis (51). Alprazolam is a medication for the treatment of anxiety and panic disorders through targeting TSPO. We found that TSPO was also overexpressed in CRC tumors, particularly in O patients, suggesting that Alprazolam might be a drug candidate for CRC treatment. Besides, we also identified some targets including ROCK1, PIN1, and ANXA5 with higher adjusted intensities in Y patients. However, the expression differences of these proteins between tumorous and nontumorous tissues were not dramatic, making them less possible to be therapeutic targets for CRC treatment.

Next, we summarized the age-associated signature proteins including DCTPP1, DHCR7, PTGES, CASP8, KIF11, PADI4, ACLY, ACOX1, SF3B3, UHRF1, JMJD6, SMARCA5, EIF4A1, and SMARCA4 with known inhibitors, which have not been evaluated in clinical trials yet (Wilcoxon rank-sum test, FDR < 0.05, median ratio (O/Y) > 1.5 or <0.67, and p value of linear correlation <0.05) (Table 1). The proteins with higher expression in normal tissues were not shown. Interestingly, all these proteins showed increased variations between tumors and normal tissues in O patients, again suggesting that the molecular differences between cancer cells and healthy cells became bigger while aging. Collectively, we identify many hallmark proteins with distinct expression in patients with CRC of different age groups, which may be clinically actionable targets for precise CRC treatment.

DISCUSSION

In summary, we for the first time presented the age-associated proteomic signatures of CRC and achieved some important findings. First, we disclosed the hallmark pathways of patients with CRC across age groups. MYC targets V1/V2 genes involved in cell growth, apoptosis, and metabolism were highly expressed in O patients with CRC. Enhanced expression of these genes usually promotes a malignant phenotype. Second, we identified plenty of proteins such as NOC2L, CCDC51, NOP2, NOC2L, NOL7, CDK5RAP1, RRP1B, CSE1L, NHP2, PPAN, and CDK1 with the adjusted intensities positively correlated with age. Higher NHP2 expression in tumors, particularly in O patients with CRC,

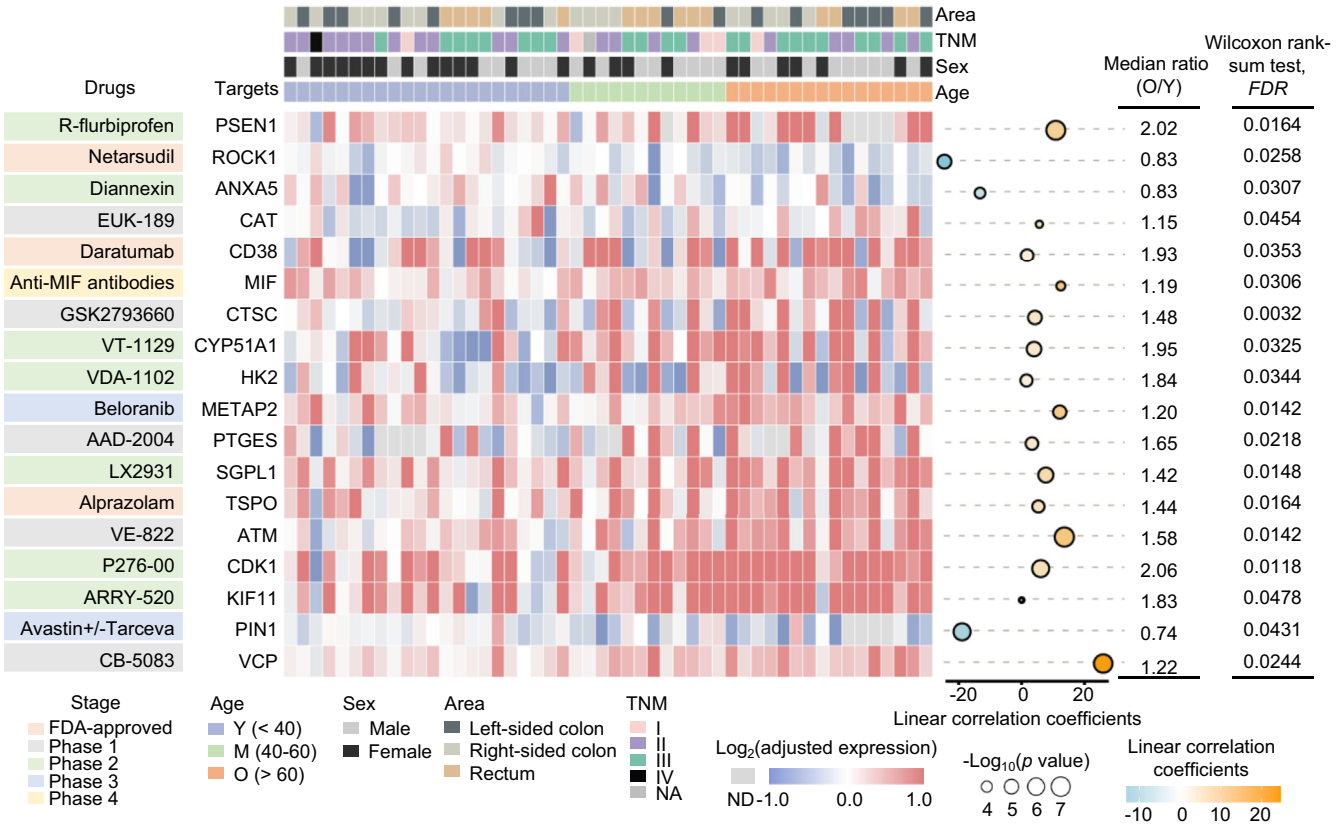

FIG. 6. **Age-associated clinically actionable targets with approved drugs or drugs in clinical trials.** Age-associated clinically actionable targets are summarized (Wilcoxon rank-sum test, FDR < 0.05, and $p < 0.05$ for linear regression). The TNM stage, lesion location, sex, and age of patients are annotated above the heatmap. The heatmap depicts the adjusted intensities of functional proteins with log2 transformation. The bubble chart describes the coefficients with age. The approved drugs or drugs in clinical trials are shown at the *left side* of the heatmap. FDR, false discovery rate.

predicts worse prognosis. Reduced NHP2 effectively arrested the cell proliferation. Third, we revealed some potential clinically actionable targets with approved drugs or drugs in clinical trials such as PSEN1, TSPO, and CDK1 showing obvious and significant expression differences between Y and O patients, as well as between tumors and the adjacent nontumorous tissues.

Cell division rates in healthy human tissues are consistently and markedly slowed down with age (52). Accordingly, cancers also grow slower in the elderly than in the Y ones because of a slower rate of cell development in the bodies of O persons (53). During the tumorigenesis, cancer cells gain more and more mutations and might compete with surrounding cells and gradually cause adjacent tissues destructed (54). Besides, the proteomic profiles of tumors also gradually change and become distinct from those of normal tissues. Huge expression difference of a target between the cancer cells and healthy cells will help increase the efficacy of treatment (22). In O patients with CRC, the molecular differences, especially the expression differences of MYC targets V1/V2, E2F targets, and G2M checkpoint gene sets associated with cancer cell proliferation and tumor metastasis, between cancerous and normal tissues, are more variable than that in the Y patients, indicating that targeting these proteins might be a better choice for CRC treatment of O patients.

Aging causes functional decline of organs and is a major risk factor for the development of cancer. Although clinical outcomes of patients with CRC across age groups have been observed for long time, age-dependent precise treatment of CRC is still less investigated. Owing to the distinct proteomic profiles of patients with CRC of different ages, some approved drugs might be only useful for the patients of a certain age group. The discovery of age-associated clinically actionable targets of CRC might help the doctors make a precision decision during CRC treatment.

TABLE 1
Age-associated potential drug targets with known inhibitors

Protein ID	Gene name	Number of unique peptides	*p* Values for linear correlation with age	Linear correlation coefficient	Median-adjusted expression (Y)	Median-adjusted expression (O)	Wilcoxon rank-sum test, FDR	Median ratio (O/Y)	Known inhibitors
Q9H773	DCTPP1	5	0.0033	6.3526	1.074	2.4213	0.015	2.25	Pyrcoumin
Q9UBM7	DHCR7	5	0.0024	8.1781	1.3192	2.8202	0.0158	2.14	AY9944; Tamoxifen
O14684	PTGES	2	0.0256	6.3371	0.8577	1.4157	0.0137	1.65	Celecoxib
Q14790	CASP8	2	0.0012	11.6687	1.1975	2.1555	0.0016	1.8	Z-IETD-FMK
P52732	KIF11	6	0.1484	3.7177	1.2844	2.3489	0.0479	1.83	Monastrol; HR22C16; CK0106023
Q9UM07	PADI4	2	0.0479	5.167	2.0944	3.365	0.002	1.61	GSK484
P53396	ACLY	44	0.0004	16.0588	1.1942	2.037	0.0007	1.71	NDI-091143; MEDICA16
Q15067	ACOX1	8	0.0011	7.4954	0.8315	1.5073	0.005	1.81	10,12-Tricosadiynoic acid
Q15393	SF3B3	34	0.0004	16.4427	1.1832	1.9397	0.0007	1.64	FR901464
Q96T88	UHRF1	9	0.0462	5.9103	1.6913	2.603	0.0417	1.54	NSC232003
O60264	SMARCA5	23	0.0059	12.648	1.2707	1.9489	0.005	1.53	ED2-AD101
P60842	EIF4A1	9	0.0024	18.8022	1.0998	1.6956	0.002	1.54	eFT226
P51532	SMARCA4	9	0.0027	14.3491	1.1898	1.8326	0.0023	1.54	PFI-3

The differentially expressed age-associated potential drug targets with known inhibitors are summarized (Wilcoxon rank-sum test, FDR < 0.05, median ratio (O/Y) >1.5 or <0.667, and $p < 0.05$ for linear regression).

DATA AVAILABILITY

The mass spectrometry raw data, the MaxQuant software, and the whole txt files have been deposited into the ProteomeXchange Consortium (http://proteomecentral.proteomexchange.org) *via* the iProX partner repository with a dataset identifier of PXD022714 (15).

Supplemental data—This article contains supplemental data.

Acknowledgments—This work was supported by the National Key R&D Program of China (No. 2018YFC2000305 and 2018YFC1312301), National Natural Science Foundation of China (No. 81570060, 31870826, and 82073221), and National Clinical Research Center for Geriatrics of West China Hospital (No. Z20191001), and West China Hospital 135 project (No. ZYYC20007, ZYGD20006, and 2016105).

Author contributions—L. D. and Z. Z. methodology; L. D. and Z. Z. writing–original draft; Y. G., Yu Liu, Z. L., T. W., and L. G. investigation; Yuan Li, H. C., Y. S., and H. X. formal analysis.

Conflict of interest—The authors declare no competing interests.

Abbreviations—The abbreviations used are: CRC, colorectal cancer; FDR, false discovery rate; GSEA, gene set enrichment analysis; IHC, immunohistochemical; M, middle-aged; O, aged; OS, overall survival; TCGA, The Cancer Genome Atlas; TMT, tandem mass tag; Y, young.

Received November 23, 2020, and in revised from, May 4, 2021
Published, MCPRO Papers in Press, June 12, 2021, https://doi.org/10.1016/j.mcpro.2021.100115

REFERENCES

1. Keum, N., and Giovannucci, E. (2019) Global burden of colorectal cancer: Emerging trends, risk factors and prevention strategies. *Nat. Rev. Gastroenterol. Hepatol.* **16**, 713–732
2. Jarosz, M., Sekuła, W., and Rychlik, E. (2013) Trends in dietary patterns, alcohol intake, tobacco smoking, and colorectal cancer in Polish population in 1960–2008. *Biomed. Res. Int.* **2013**, 183204
3. Araghi, M., Soerjomataram, I., Bardot, A., Ferlay, J., Cabasag, C. J., Morrison, D. S., De, P., Tervonen, H., Walsh, P. M., Bucher, O., Engholm, G., Jackson, C., McClure, C., Woods, R. R., Saint-Jacques, N., *et al*. (2019) Changes in colorectal cancer incidence in seven high-income countries: A population-based study. *Lancet Gastroenterol. Hepatol.* **4**, 511–518
4. McKay, A., Donaleshen, J., Helewa, R. M., Park, J., Wirtzfeld, D., Hochman, D., Singh, H., and Turner, D. (2014) Does young age influence the prognosis of colorectal cancer: A population-based analysis. *World J. Surg. Oncol.* **12**, 370
5. Ballester, V., Rashtak, S., and Boardman, L. (2016) Clinical and molecular features of young-onset colorectal cancer. *World J. Gastroenterol.* **22**, 1736–1744
6. Lieu, C. H., Golemis, E. A., Serebriiskii, I. G., Newberg, J., Hemmerich, A., Connelly, C., Messersmith, W. A., Eng, C., Eckhardt, S. G., Frampton, G., Cooke, M., and Meyer, J. E. (2019) Comprehensive genomic landscapes in early and later onset colorectal cancer. *Clin. Cancer Res.* **25**, 5852–5858
7. Jiang, Y., Sun, A., Zhao, Y., Ying, W., Sun, H., Yang, X., Xing, B., Sun, W., Ren, L., Hu, B., Li, C., Zhang, L., Qin, G., Zhang, M., Chen, N., *et al*. (2019) Proteomics identifies new therapeutic targets of early-stage hepatocellular carcinoma. *Nature* **567**, 257–261
8. Xu, J.-Y., Zhang, C., Wang, X., Zhai, L., Ma, Y., Mao, Y., Qian, K., Sun, C., Liu, Z., Jiang, S., Wang, M., Feng, L., Zhao, L., Liu, P., Wang, B., *et al*. (2020) Integrative proteomic characterization of human lung adenocarcinoma. *Cell* **182**, 245–261.e217
9. Gao, Q., Zhu, H., Dong, L., Shi, W., Chen, R., Song, Z., Huang, C., Li, J., Dong, X., Zhou, Y., Liu, Q., Ma, L., Wang, X., Zhou, J., Liu, Y., *et al*. (2019) Integrated proteogenomic characterization of HBV-related hepatocellular carcinoma. *Cell* **179**, 561–577.e522
10. Ge, S., Xia, X., Ding, C., Zhen, B., Zhou, Q., Feng, J., Yuan, J., Chen, R., Li, Y., Ge, Z., Ji, J., Zhang, L., Wang, J., Li, Z., Lai, Y., *et al*. (2018) A proteomic landscape of diffuse-type gastric cancer. *Nat. Commun.* **9**, 1012
11. Zhang, B., Wang, J., Wang, X., Zhu, J., Liu, Q., Shi, Z., Chambers, M. C., Zimmerman, L. J., Shaddox, K. F., Kim, S., Davies, S. R., Wang, S., Wang, P., Kinsinger, C. R., Rivers, R. C., *et al*. (2014) Proteogenomic characterization of human colon and rectal cancer. *Nature* **513**, 382–387
12. Vasaikar, S., Huang, C., Wang, X., Petyuk, V. A., Savage, S. R., Wen, B., Dou, Y., Zhang, Y., Shi, Z., Arshad, O. A., Gritsenko, M. A., Zimmerman, L. J., McDermott, J. E., Clauss, T. R., Moore, R. J., *et al*. (2019) Proteogenomic analysis of human colon cancer reveals new therapeutic opportunities. *Cell* **177**, 1035–1049.e1019
13. Sethi, M. K., Thaysen-Andersen, M., Kim, H., Park, C. K., Baker, M. S., Packer, N. H., Paik, Y. K., Hancock, W. S., and Fanayan, S. (2015) Quantitative proteomic analysis of paired colorectal cancer and non-tumorigenic tissues reveals signature proteins and perturbed pathways involved in CRC progression and metastasis. *J. Proteomics* **126**, 54–67
14. Li, C., Sun, Y. D., Yu, G. Y., Cui, J. R., Lou, Z., Zhang, H., Huang, Y., Bai, C. G., Deng, L. L., Liu, P., Zheng, K., Wang, Y. H., Wang, Q. Q., Li, Q. R., Wu, Q. Q., *et al*. (2020) Integrated omics of metastatic colorectal cancer. *Cancer Cell* **38**, 734–747.e9
15. Ma, J., Chen, T., Wu, S., Yang, C., Bai, M., Shu, K., Li, K., Zhang, G., Jin, Z., He, F., Hermjakob, H., and Zhu, Y. (2019) iProX: An integrated proteome resource. *Nucleic Acids Res.* **47**, D1211–D1217
16. Deutsch, E. W., Lane, L., Overall, C. M., Bandeira, N., Baker, M. S., Pineau, C., Moritz, R. L., Corrales, F., Orchard, S., Van Eyk, J. E., Paik, Y. K., Weintraub, S. T., Vandenbrouck, Y., and Omenn, G. S. (2019) Human proteome project mass spectrometry data interpretation guidelines 3.0. *J. Proteome Res.* **18**, 4108–4116
17. Lambert, S. A., Jolma, A., Campitelli, L. F., Das, P. K., Yin, Y., Albu, M., Chen, X., Taipale, J., Hughes, T. R., and Weirauch, M. T. (2018) The human transcription factors. *Cell* **172**, 650–665
18. Uhlén, M., Fagerberg, L., Hallström, B. M., Lindskog, C., Oksvold, P., Mardinoglu, A., Sivertsson, Å., Kampf, C., Sjöstedt, E., Asplund, A., Olsson, I., Edlund, K., Lundberg, E., Navani, S., Szigyarto, C. A., *et al*. (2015) Proteomics. Tissue-based map of the human proteome. *Science* **347**, 1260419
19. Straub, R. H. (2020) The memory of the fatty acid system. *Prog. Lipid Res.* **79**, 101049
20. Sim, L., Willemsma, C., Mohan, S., Naim, H. Y., Pinto, B. M., and Rose, D. R. (2010) Structural basis for substrate selectivity in human maltase-glucoamylase and sucrase-isomaltase N-terminal domains. *J. Biol. Chem.* **285**, 17763–17770
21. Wu, L., Candille, S. I., Choi, Y., Xie, D., Jiang, L., Li-Pook-Than, J., Tang, H., and Snyder, M. (2013) Variation and genetic control of protein abundance in humans. *Nature* **499**, 79–82
22. Blagosklonny, M. V., and Pardee, A. B. (2001) Exploiting cancer cell cycling for selective protection of normal cells. *Cancer Res.* **61**, 4301–4305
23. Kosi, N., Alić, I., Kolačević, M., Vrsaljko, N., Jovanov Milošević, N., Sobol, M., Philimonenko, A., Hozák, P., Gajović, S., Pochet, R., and Mitrečić, D. (2015) Nop2 is expressed during proliferation of neural stem cells and in adult mouse and human brain. *Brain Res.* **1597**, 65–76
24. Behrens, P., Brinkmann, U., and Wellmann, A. (2003) CSE1L/CAS: Its role in proliferation and apoptosis. *Apoptosis* **8**, 39–44
25. Pimiento, J. M., Neill, K. G., Henderson-Jackson, E., Eschrich, S. A., Chen, D.-T., Husain, K., Shibata, D., Coppola, D., and Malafa, M. P. (2016) Knockdown of CSE1L gene in colorectal cancer reduces tumorigenesis *in vitro*. *Am. J. Pathol.* **186**, 2761–2768
26. Li, J., Wang, Y., Wang, X., and Yang, Q. (2020) CDK1 and CDC20 overexpression in patients with colorectal cancer are associated with poor prognosis: Evidence from integrated bioinformatics analysis. *World J. Surg. Oncol.* **18**, 50

27. Wu, C. X., Wang, X. Q., Chok, S. H., Man, K., Tsang, S. H. Y., Chan, A. C. Y., Ma, K. W., Xia, W., and Cheung, T. T. (2018) Blocking CDK1/PDK1/β-catenin signaling by CDK1 inhibitor RO3306 increased the efficacy of sorafenib treatment by targeting cancer stem cells in a preclinical model of hepatocellular carcinoma. *Theranostics* **8**, 3737–3750
28. Klein, A. P., Wolpin, B. M., Risch, H. A., Stolzenberg-Solomon, R. Z., Mocci, E., Zhang, M., Canzian, F., Childs, E. J., Hoskins, J. W., Jermusyk, A., Zhong, J., Chen, F., Albanes, D., Andreotti, G., Arslan, A. A., *et al*. (2018) Genoe-wide meta-analysis identifies five new susceptibility loci for pancreatic cancer. *Nat. Commun.* **9**, 556
29. Shay, J. W. (2016) Role of telomeres and telomerase in aging and cancer. *Cancer Discov.* **6**, 584–593
30. Shay, J. W., and Wright, W. E. (2019) Telomeres and telomerase: Three decades of progress. *Nat. Rev. Genet.* **20**, 299–309
31. Mender, I., LaRanger, R., Luitel, K., Peyton, M., Girard, L., Lai, T. P., Batten, K., Cornelius, C., Dalvi, M. P., Ramirez, M., Du, W., Wu, L. F., Altschuler, S. J., Brekken, R., Martinez, E. D., *et al*. (2018) Telomerase-mediated strategy for overcoming non-small cell lung cancer targeted therapy and chemotherapy resistance. *Neoplasia* **20**, 826–837
32. Shay, J. W., and Wright, W. E. (2006) Telomerase therapeutics for cancer: Challenges and new directions. *Nat. Rev. Drug Discov*. **5**, 577–584
33. Vulliamy, T., Beswick, R., Kirwan, M., Marrone, A., Digweed, M., Walne, A., and Dokal, I. (2008) Mutations in the telomerase component NHP2 cause the premature ageing syndrome dyskeratosis congenita. *Proc. Natl. Acad. Sci. U. S. A.* **105**, 8073–8078
34. Bushweller, J. H. (2019) Targeting transcription factors in cancer — from undruggable to reality. *Nat. Rev. Cancer* **19**, 611–624
35. Li, C., Bu, J., Liao, Y., Zhang, J., Han, J., Zhang, H., Xing, H., Li, Z., Wu, H., Liang, L., Wang, M., Qin, W., and Yang, T. (2018) High expressions of CUL4A and TP53 in colorectal cancer predict poor survival. *Cell Physiol. Biochem.* **51**, 2829–2842
36. Jiang, M., Zhuang, H., Xia, R., Gan, L., Wu, Y., Ma, J., Sun, Y., and Zhuang, Z. (2017) KIF11 is required for proliferation and self-renewal of docetaxel resistant triple negative breast cancer cells. *Oncotarget* **8**, 92106–92118
37. Wen, J., Min, X., Shen, M., Hua, Q., Han, Y., Zhao, L., Liu, L., Huang, G., Liu, J., and Zhao, X. (2019) ACLY facilitates colon cancer cell metastasis by CTNNB1. *J. Exp. Clin. Cancer Res.* **38**, 401
38. Chen, K., Xiao, H., Zeng, J., Yu, G., Zhou, H., Huang, C., Yao, W., Xiao, W., Hu, J., Guan, W., Wu, L., Huang, J., Huang, Q., Xu, H., and Ye, Z. (2017) Alternative splicing of EZH2 pre-mRNA by SF3B3 contributes to the tumorigenic potential of renal cancer. *Clin. Cancer Res.* **23**, 3428–3441
39. Kong, X., Chen, J., Xie, W., Brown, S. M., Cai, Y., Wu, K., Fan, D., Nie, Y., Yegnasubramanian, S., Tiedemann, R. L., Tao, Y., Chiu Yen, R. W., Topper, M. J., Zahnow, C. A., Easwaran, H., *et al*. (2019) Defining UHRF1 domains that support maintenance of human colon cancer DNA methylation and oncogenic properties. *Cancer Cell* **35**, 633–648.e637
40. Jin, J., Yu, Q., Han, C., Hu, X., Xu, S., Wang, Q., Wang, J., Li, N., and Cao, X. (2013) LRRFIP2 negatively regulates NLRP3 inflammasome activation in macrophages by promoting Flightless-I-mediated caspase-1 inhibition. *Nat. Commun.* **4**, 2075
41. Moossavi, M., Parsamanesh, N., Bahrami, A., Atkin, S. L., and Sahebkar, A. (2018) Role of the NLRP3 inflammasome in cancer. *Mol. Cancer* **17**, 158
42. Furukawa, D., Chijiwa, T., Matsuyama, M., Mukai, M., Matsuo, E. I., Nishimura, O., Kawai, K., Suemizu, H., Hiraoka, N., Nakagohri, T., Yasuda, S., and Nakamura, M. (2014) Zinc finger protein 185 is a liver metastasis-associated factor in colon cancer patients. *Mol. Clin. Oncol.* **2**, 709–713
43. Wei, Z., Ma, W., Qi, X., Zhu, X., Wang, Y., Xu, Z., Luo, J., Wang, D., Guo, W., Li, X., Xin, S., Yu, J., and Li, G. (2016) Pinin facilitated proliferation and metastasis of colorectal cancer through activating EGFR/ERK signaling pathway. *Oncotarget* **7**, 29429–29439
44. Stupack, D. G. (2013) Caspase-8 as a therapeutic target in cancer. *Cancer Lett.* **332**, 133–140
45. Guerrero-Martínez, J. A., and Reyes, J. C. (2018) High expression of SMARCA4 or SMARCA2 is frequently associated with an opposite prognosis in cancer. *Sci. Rep.* **8**, 2043
46. Habets, R. A., de Bock, C. E., Serneels, L., Lodewijckx, I., Verbeke, D., Nittner, D., Narlawar, R., Demeyer, S., Dooley, J., Liston, A., Taghon, T., Cools, J., and de Strooper, B. (2019) Safe targeting of T cell acute lymphoblastic leukemia by pathology-specific NOTCH inhibition. *Sci. Transl. Med.* **11**, eaau6246
47. Suman, S., Das, T. P., Ankem, M. K., and Damodaran, C. (2014) Targeting Notch signaling in colorectal cancer. *Curr. Colorectal Cancer Rep.* **10**, 411–416
48. Santamaría, D., Barrière, C., Cerqueira, A., Hunt, S., Tardy, C., Newton, K., Cáceres, J. F., Dubus, P., Malumbres, M., and Barbacid, M. (2007) Cdk1 is sufficient to drive the mammalian cell cycle. *Nature* **448**, 811–815
49. Kang, J., Sergio, C. M., Sutherland, R. L., and Musgrove, E. A. (2014) Targeting cyclin-dependent kinase 1 (CDK1) but not CDK4/6 or CDK2 is selectively lethal to MYC-dependent human breast cancer cells. *BMC Cancer* **14**, 32
50. van de Donk, N. W. C. J., Richardson, P. G., and Malavasi, F. (2018) CD38 antibodies in multiple myeloma: Back to the future. *Blood* **131**, 13–29
51. Rupprecht, R., Papadopoulos, V., Rammes, G., Baghai, T. C., Fan, J., Akula, N., Groyer, G., Adams, D., and Schumacher, M. (2010) Translocator protein (18 kDa) (TSPO) as a therapeutic target for neurological and psychiatric disorders. *Nat. Rev. Drug Discov.* **9**, 971–988
52. Tomasetti, C., Poling, J., Roberts, N. J., London, N. R., Pittman, M. E., Haffner, M. C., Rizzo, A., Baras, A., Karim, B., Kim, A., Heaphy, C. M., Meeker, A. K., Hruban, R. H., Iacobuzio-Donahue, C. A., and Vogelstein, B. (2019) Cell division rates decrease with age, providing a potential explanation for the age-dependent deceleration in cancer incidence. *Proc. Natl. Acad. Sci. U. S. A.* **116**, 20482–20488
53. Estapé, T. (2018) Cancer in the elderly: Challenges and barriers. *Asia Pac. J. Oncol. Nurs.* **5**, 40–42
54. Suijkerbuijk, S. J. E., Kolahgar, G., Kucinski, I., and Piddini, E. (2016) Cell competition drives the growth of intestinal adenomas in Drosophila. *Curr. Biol.* **26**, 428–438